An analysis of a Tikhonov regularized Gauss-Newton reconstruction approach to GPR tomography

Naren Naik, Hichem Sahli
ETRO-Department, IRIS-Research Group
Vrije Universiteit Brussel
Brussel, BELGIUM
nnaik@etro.vub.ac.be, hsahli@etro.vub.ac.be

Jerry Eriksson
Department of Computing Science
Umeå University
Umeå, SWEDEN
Jerry.Eriksson@cs.umu.se

***Abstract*— The present work is about the application of a Tikhonov regularized Gauss-Newton scheme to the solution of the nonlinear minimum norm reconstruction problem of GPR tomography, with the aims of (a) setting of a regularization parameter sequence to achieve convergence, (b) evaluation of an iteration matrix at a given nominal parameter estimate, and (c) study the effects of curvatures in parameter and objective-function spaces on the convergence.**

Keywords-GPR Tomography ; almost rank deficient problems ; nonlinear inverse problems; Gauss-Newton method .

I. INTRODUCTION

A. *The GPR tomography problem*

The inverse scattering problem being presently considered is to recover a subsurface object's electrical permittivity ($\varepsilon(\mathbf{r})$, $\mathbf{r} \in \mathbf{R}^2$), and conductivity ($\sigma(\mathbf{r})$, $\mathbf{r} \in \mathbf{R}^2$), from the measurements at various frequencies, on a receiver surface outside the object, of the scattered field obtained from the interaction of an incident radiation with the object in question. In the present work, the scattering process in GPR tomography is assumed to be modelled (in the scalar approximation) by the 2D Helmholtz equation. The Helmholtz equation for the complex amplitude $u(\mathbf{r},\mathbf{r}_n,\omega)$ at a point $\mathbf{r}=(x,z)$, of a monochromatic wave of angular frequency ω, due to a source at $\mathbf{r}_n$, propagating through a medium of complex wave number $k(\mathbf{r},\omega)$, is given by

$$\Delta u(\mathbf{r},\mathbf{r}_n,\omega) + k^2(\mathbf{r},\omega)\, u(\mathbf{r},\mathbf{r}_n,\omega) = j_n(\mathbf{r}_n,\omega) \qquad (1)$$

where, Δ is the Laplacian operator, $j_n(\mathbf{r}_n,\omega)$ is the assumed current distribution corresponding to the n-th transmitter. The fields $u(\mathbf{r},\mathbf{r}_n,\omega)$ are assumed to be outgoing and satisfying the Sommerfeld radiation conditions at infinity. The complex wave-number, $k(\mathbf{r},\omega)$, is given by

$$k^2(\mathbf{r},\omega) = \omega^2\mu_0\,\varepsilon(\mathbf{r})\,(1+i\;\sigma(\mathbf{r},\omega)/(\omega\,\varepsilon(\mathbf{r}))) \qquad (2)$$

where μ_0 is the magnetic permeability of free space.

B. *Setting and brief of present work*

Major reconstruction approaches [1],[2], [3] in diffraction tomography either utilize (a) the linearised Born or Rytov approximation solutions to the scattered fields, or, (b) the partially nonlinear Born iterative type approach wherein the interior fields inside the objects at each iteration are kept fixed at those estimated at the previous step, or, (c) the nonlinear distorted-Born/Newton-Kantorovich or contrast-source-inversion methods, wherein the interior fields are predicted at the present step based upon the integral equation model of scattering.

Typically, nonlinear optimization based schemes such as the Gauss-Newton/Newton-Kantorovich or conjugate-gradient methods are employed to solve the above reconstruction problem. The present work is about the application and analysis of a Tikhonov regularized Gauss-Newton (GN) scheme to the solution and analysis of the nonlinear minimum norm reconstruction problem of GPR tomography, in the light of a perturbation-theory based framework [4] of Jerry Eriksson and Per-Åke Wedin for almost rank-deficient problems, that measures both parameter and function space curvatures, which reveal not only some characteristics of the problem, but also the predicted efficiency of the GN-method.

The layout of the paper is as follows. Section 2 outlines the Tikhonov regularized GN scheme to solve the reconstruction problem. In the analysis phase, the iteration matrix at a point close to the solution point is given in section 3, as are the curvatures in the parameter and objective function spaces, and their implications. Section 4 treats the numerical experiments on reconstructions, and, section 5 presents the conclusions.

II. TIKHONOV REGULARIZED GN RECONSTRUCTION SCHEME

The nonlinear reconstruction problem of GPR tomography can be stated as the solution to the following nonlinear minimum norm problem

$$\min_{\mathbf{f}} \|\mathbf{f}-\mathbf{c}\|_2^2 \text{ such that } (1/2)\|\zeta(\mathbf{f})\|_2^2 \text{ is minimal} \qquad (3)$$

where $\mathbf{f}$ is the row-ordered object parameter vector, with pointwise values corresponding to

$$f(\mathbf{r})=(k^2(\mathbf{r},\omega)-k_{amb}^2(\mathbf{r},\omega))/\,k_{amb}^2(\mathbf{r},\omega) \qquad (4)$$

This work is supported by VUB research council - Concerted Action project GOA20 "Numercial issues in tomographic shallow subsurface imaging" .

with $k(\mathbf{r},\omega)$ being the wave-number in the actual physical setting of the object(s) of interest embedded in an ambient medium corresponding to a wave-number $k_{amb}(\mathbf{r},\omega)$, $\mathbf{c}$ being a known constant, and,

$$\zeta(\mathbf{f})=\mathbf{g}-\mathbf{A}(\mathbf{f}) \quad (5)$$

where $\mathbf{g}$ is the concatenated measured scattered field data for a frequency set, and, $\mathbf{A}(\mathbf{f})$ is the measurement functional corresponding to the tomographic process, obtained in the present work via the integral equation framework of scattering, using the method of moments [5].

To solve the above minimum norm problem, an iterative scheme based upon the GN approximation is utilized. The multi-frequency GPR tomography problem has an almost rank-deficient Jacobian matrix (w.r.t $\zeta(\mathbf{f})$) $\mathbf{J}(\mathbf{f})$ of at the solution point of $\zeta(\mathbf{f})\approx 0$. It is well-known that the GN-method is a very efficient approach for many parameter estimation problems. However, for ill-conditioned inverse problems, the curvatures become too large, and first order methods such as the GN-method will not converge. Using Tikhonov regularization, a stable solution may be found which greatly improves the condition of the problem and also the convergence rate for the GN-method. The corresponding Tikhonov regularized (with regularization parameter μ) nonlinear least-squares problem is

$$\min_{\mathbf{f}} \| (\zeta(\mathbf{f}), \mu(\mathbf{f}-\mathbf{c}))^T\|_2^2 \quad (6)$$

To solve this problem, an iterative scheme based upon the GN approximation solves, at the current iterate $\mathbf{f}$,

$$\min_{\mathbf{p}} \| (\mathbf{J}(\mathbf{f})\mathbf{p} + \zeta(\mathbf{f}), \mu(\mathbf{f}-\mathbf{c}+\mathbf{p}))^T\|_2^2 \quad (7)$$

The next iterate is given by $\mathbf{f}^{k+1} = \mathbf{f}^k + \alpha_k \mathbf{p}^k$, where the step-length α_k is chosen such that the objective functional is sufficiently reduced. The search direction $\mathbf{p}$ computed from (7) can be written as

$$\mathbf{p} = -\mathbf{B}\,(\zeta(\mathbf{f}^k), \mathbf{f}^k - \mathbf{c})^T \quad (8)$$

with the matrix $\mathbf{B}=((\mathbf{J}^T\mathbf{J} + \mu^2\mathbf{I})^{-1}\mathbf{J}^T, \mu^2(\mathbf{J}^T\mathbf{J} + \mu^2\mathbf{I})^{-1})$.

III. Local Convergence of the Tikhonov Regularized GN Scheme

In this section, the Tikhonov regularized GN scheme is analyzed for convergence by evaluating an iteration matrix at the current iterate, which is then subsequently decomposed to yield contributions to the rate of convergence from various sources. The analysis in what follows is on the lines of that in [4].

A. The local iteration/convergence matrix

The objective is to study the local convergence of a method defined by

$$\mathbf{f}^{k+1} = \mathbf{f}^k - \mathbf{B}_k\ \mathbf{h}(\mathbf{f}^k), \text{ where } \mathbf{h}(\mathbf{f})=(\zeta(\mathbf{f}), \mu\,(\mathbf{f}-\mathbf{c}))^T \quad (9)$$

Note that (a) $\mathbf{B}\,(\mathbf{J}, \mathbf{I})^T = \mathbf{I}$, and, (b) if $\mathbf{f}_0$ is a fixed point of the above algorithm, then $\mathbf{B}(\mathbf{f}_0)\mathbf{h}(\mathbf{f}_0)=0$ is satisfied.

Making a series expansion of $\mathbf{h}(\mathbf{f}_0)$ around $\mathbf{h}(\mathbf{f}^k)$, we get

$$\mathbf{h}(\mathbf{f}_0)= \mathbf{h}(\mathbf{f}^k) + (\mathbf{J}, \mathbf{I})^T (\mathbf{f}_0 - \mathbf{f}^k) + O(\|\mathbf{f}_0 - \mathbf{f}^k\|_2^2) \quad (10)$$

Thus it follows that upto 1st order terms

$$\mathbf{B}_k\,\mathbf{h}(\mathbf{f}_0)= \mathbf{B}_k\,\mathbf{h}(\mathbf{f}^k) + (\mathbf{f}_0 - \mathbf{f}^k) \quad (11)$$

Hence from (9),

$$\mathbf{f}^{k+1}-\mathbf{f}_0 \;=\; -\,(\mathbf{B}_k - \mathbf{B}(\mathbf{f}_0))\mathbf{h}(\mathbf{f}_0) + 2^{nd}\text{order terms}$$

It can be obtained that

$$-(\mathbf{B}_k - \mathbf{B}(\mathbf{f}_0))\mathbf{h}(\mathbf{f}_0)= -\,(\mathbf{J}^T\mathbf{J} + \mu^2\mathbf{I})^{-1}(\delta\mathbf{J})^T\,\mathbf{f}_0 \quad (12)$$

where

$$\delta\mathbf{J} = \mathbf{J} - \mathbf{J}_0 = ((\mathbf{f}^k - \mathbf{f}_0)^T\,\mathbf{H}_1\ \ldots\ (\mathbf{f}^k - \mathbf{f}_0)^T\,\mathbf{H}_m)^T \quad (13)$$

with $\mathbf{H}_i \equiv \ddot{\zeta}_i(\mathbf{f}^k)$, the Hessian matrix corresponding to the i-th measurement. Hence, we can write

$$\mathbf{f}^{k+1}-\mathbf{f}_0 = \mathbf{K}(\mathbf{f}^k)\,(\mathbf{f}^k - \mathbf{f}_0) + 2^{nd}\text{ order terms} \quad (14)$$

where the spectral radius of the local iteration matrix $\mathbf{K}(\mathbf{f}^k)$ determines the rate of convergence.

B. Decomposition of the convergence matrix

Define the singular value decomposition of the Jacobian matrix, $\mathbf{J}$, in the form $\mathbf{J} = \mathbf{J}_1 + \mathbf{J}_2$, as follows

$$\mathbf{J}=\mathbf{U}\,\mathbf{S}\,\mathbf{V}^T = (\mathbf{U}_1, \mathbf{U}_2)\,\mathrm{diag}(\mathbf{S}_1, \mathbf{S}_2)\,(\mathbf{V}_1, \mathbf{V}_2)^T \quad (15)$$

with $\mathbf{S}_1=\mathrm{diag}(\sigma_1, \ldots, \sigma_r)$, and $\mathbf{S}_2 =\mathrm{diag}(\sigma_{r+1}, \ldots, \sigma_n)$, where r is a rank of interest at a particular iteration, usually considered as the number of singular values above the value of μ.

First, splitting $(\mathbf{J}^T\mathbf{J} + \mu^2\mathbf{I})^{-1}$ into terms corresponding to the subspaces defined by the assumed value of r, we have

$$\mu^2\,(\mathbf{J}^T\mathbf{J} + \mu^2\mathbf{I})^{-1} = \mu^2\,\mathbf{V}_1\,\mathbf{S}_{V1}\,\mathbf{V}_1^T + \mathbf{V}_2\,\mathbf{S}_{V2}\,\mathbf{V}_2^T \equiv \mu^2\,\mathbf{E}(\mu) + \mathbf{N}(\mu) \quad (16)$$

where $\mathbf{S}_{V1} \equiv \mathrm{diag}\{1/[\sigma_1^2(1+(\mu/\sigma_1)^2)], \ldots, 1/[\sigma_r^2(1+(\mu/\sigma_r)^2)]\}$, and $\mathbf{S}_{V2} \equiv \mathrm{diag}\{1/[1+(\sigma_{r+1}/\mu)^2], \ldots, 1/[1+(\sigma_n/\mu)^2]\}$.

Defining $R_1 \equiv \mathrm{Range}(\mathbf{J}_1)$, $S_1 \equiv \text{Null-space}(\mathbf{J}_1^T)$, $M_1 \equiv \mathrm{Range}(\mathbf{J}_1^T)$ and $N_1 \equiv \text{Null-space}(\mathbf{J}_1)$, we observe that at a solution, $\mathbf{J}^T\zeta + \mu^2\,(\mathbf{f}-\mathbf{c}) = 0$, and thus $\mathbf{J}_1^T\zeta + \mu^2\,P_{M1}(\mathbf{f}-\mathbf{c}) = 0$, where P_{M1} is the orthogonal projector onto M_1. We thus have

$$\zeta \equiv \zeta(\mathbf{f}) = P_{R1}\zeta + P_{S1}\zeta = -\,\mu^2\,(\mathbf{J}_1^+)^T(\mathbf{f}-\mathbf{c}) + P_{S1}\zeta\,.$$

Hence we obtain from (12), (13), (14) and (16),

$$\mathbf{K}(\mathbf{f}) = \mathbf{K}_1(\mathbf{f}) + \mathbf{K}_2(\mathbf{f}) + \mathbf{K}_3(\mathbf{f}) + \mathbf{K}_4(\mathbf{f}) \quad (17)$$

where

$$\mathbf{K}_1(\mathbf{f}) = -\mathbf{E}(\mu)\,\mathbf{H}^T\!\natural\, P_{S1}\zeta\,,\ \mathbf{K}_2(\mathbf{f}) = \mathbf{N}(\mu)\,\mathbf{H}^T\!\natural\,((\mathbf{J}_1^+)^T(\mathbf{f}-\mathbf{c}))$$

$$\mathbf{K}_3(\mathbf{f}) = \mathbf{E}(\mu)\,\mathbf{H}^T\!\natural\,((\mathbf{J}_1^+)^T(\mathbf{f}-\mathbf{c}))\,,\ \text{and,}$$

$$\mathbf{K}_4(\mathbf{f}) = -(1/\mu^2)\,\mathbf{N}(\mu)\,\mathbf{H}^T\!\natural\, P_{S1}\zeta$$

where $\mathbf{H}^T=(\mathbf{H}_1^T, \ldots, \mathbf{H}_m^T)$, and the "inner product" $\natural$ is defined as $\mathbf{H}^T\!\natural\,\mathbf{q} \equiv \sum_i \mathbf{H}_i^T q_i$.

In the above expression for $\mathbf{K}(\mathbf{f})$, we observe that the first two terms correspond to the errors due to the normal curvatures in the objective-function and parameter spaces respectively, the third term is typically small when close to convergence, and the fourth term limits the decrease in the value of the regularization parameter.

It can be seen that the GN scheme converges iff $\rho(\mathbf{K})<1$, where $\rho(.)$ denotes the spectral radius (maximum absolute eigenvalue) of its matrix argument.

IV. SIMULATIONAL STUDIES

A. Numerical Aspects

The computational aspects related to the physical modeling of the tomographic process are the computation of the scattered fields given a nominal parameter estimate, and the corresponding Jacobian and Hessian matrices. In our work, we form the measurement equation (5) by discretizing the integral equation of scattering using a method of moments pulse-basis point-matching procedure [5]. The Green function used is the half-space Green function [6], with air and ground being the two spaces. The Jacobian and Hessian calculations are made in the "fully-nonlinear" regime wherein the interior fields are predicted at the present step taking into account their variation with the nominal estimate.

In the nonlinear optimization scheme to solve the minimum norm problem (3), the setting of the regularization parameter μ is done by initializing it to a suitably "large" value and then reducing it in steps corresponding to a reduction in objective function value in the line-search step, when the step-size is large enough (i.e., the step-size α should be close to 1).

B. Test cases

Numerical results (obtained in Matlab) are presented for two 2D shallow-sub-surface mine-like test objects of circular-cross-section (center at 4 cm depth and radius of 3.4 cm, with settings given in Table 1), embedded in a half-space (air-ground) ambient medium. Scattered data at multiple-frequencies (0.7, 0.9, 1.1, 1.3 GHz) and multiple-angle plane wave incidence (15 angles in $[-\pi/3,\pi/3]$) is used in our studies.

TABLE I. PHANTOM PARAMETERS

Phantom	Ambient (ε_r, tanδ)	Object (ε_r, tanδ), f
P1	Dry sand (2.55, 0.0282)	(4.24,0.0636) f=0.6644+i 0.0588
P2	Wet sand (4.5, 0.03)	(10,0.01797) f=1.2221-i0.02667

Reconstructions are performed for these two phantoms for exact (noiseless), and mildly noisy data (exact data is added to 0-mean Gaussian noise of std-deviation of one-tenth of its max-amplitude). The a-priori constraints used in our reconstructions are of the bound and support of the object parameters. In the exact data case, tight support constraints are used (this being a benchmarking example), while in the mildly noisy case, more relaxed support constraints are employed. Reconstructions of the real parts of the complex parameter estimates in Figs. 1,3,5,7 show acceptable reconstructions w.r.t the parameter values in Table 1. Corresponding plots of the decrease of residual and regularization parameter with iteration number are shown in Figs. 2,4,6,8.

The spectral radii of the individual components of the convergence matrix are defined as $k_i = \rho(\mathbf{K}_i)$, i=1,...,4, where $\mathbf{K}_i$ are as defined in (17). Due to paucity of space, we write results for the two phantoms in the reconstruction from exact data, in the form of vectors with entries [Iteration, μ, k1, k2, k3, k4, $\rho(\mathbf{K})$]. Corresponding to P1, we obtained [4, 0.025, 0.0026, 0.6139, 0.4461, 0.0063, 0.6858], [8, 0.00625, 0.0122, 0.5795, 0.1741, 0.0405, 0.5873], and [10, 0.00625, 0.0122, 0.5795, 0.1741, 0.0405, 0.5873], and corresponding to P2, [4, 0.05, 0.0120, 1.5126, 0.7140, 0.0328, 1.5708], [8, 0.05, 0.0120, 1.5143, 0.7136, 0.0328, 1.5725], and [10, 0.05, 0.0120, 1.5143, 0.7136, 0.0328, 1.5725].

We observe that the convergence rate component, k_1 corresponding to the objective function residual is small in both cases, indicating that the residual aspect is having a high convergence. The term k_2 being larger shows that the major influence on the lack of convergence for phantom P2 comes from the parameter space, which is quite understandable considering the higher nonlinearity in P2. Also, k_3 being large and k_4 being small indicates that the value of the regularization parameter has not attained its minimum possible value.

V. CONCLUSIONS

We have demonstrated the application and analysis of a Tikhonov regularized minimum-norm formulation of a nonlinear almost-rank-deficient reconstruction problem of GPR tomography by (a) obtaining sequences of regularization parameters that yield acceptable reconstructions for test cases considered, and, (b) better understanding the scheme's convergence behaviour by looking separately at convergence rates in parameter and objective function spaces.

ACKNOWLEDGMENT

Naren Naik thanks Professors S.M. Rao, Peter van den Berg, Giovanni Leone, Dinh Nho Hao for some very useful discussions. He thanks Bart Truyen and Luc van Kempen for pointing out some very useful references.

REFERENCES

[1] W. C. Chew, G. P. Otto, W. H. Weedon, J. H. Lin, C. C. Lu, Y. M. Wang and M. Moghaddam, "Nonlinear diffraction tomography - the use of inverse scattering for imaging," Int. J. Imaging Sys. Technol., 7: 16-24, Jan. 1996.

[2] R. F. Remis and P. M. van den Berg, "On the equivalence of the Newton-Kantorovich and distorted Born methods", Inverse Problems 16(1): L1-L4, Feb. 2000.

[3] P. M. van den Berg and A. Abubakar, "Contrast source inversion method: state of art", Progress in Electromagnetics Research, PIER 34, 189-218, 2001.

[4] J. Eriksson, Optimization and regularization of nonlinear least squares problems, Ph. D. Thesis, Department of Computing Science, Umeå University, Sweden, 1996.

[5] S. M. Rao and G. K. Gothard, "Integral equations", Wiley Encyclopedia of Electrical and Electronics, Engineering, Ed. John Webster, 351-361.

[6] M. Cheney and D. Isaacson, "Inverse problems for a perturbed dissipative half-space",Inv. Pb.,11(4):865-868, 1995.

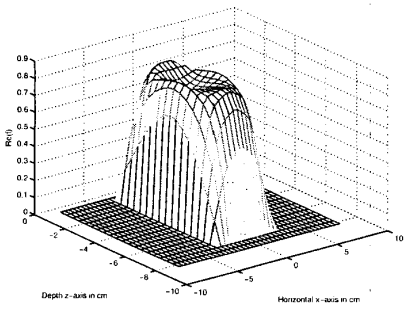

Figure 1. Plot of Re(f) vs. (x,z) for P1 with exact data

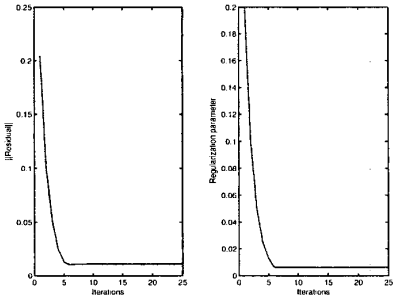

Figure 2. Plots of residual and regularization parameter vs. iteration for P1 with exact data

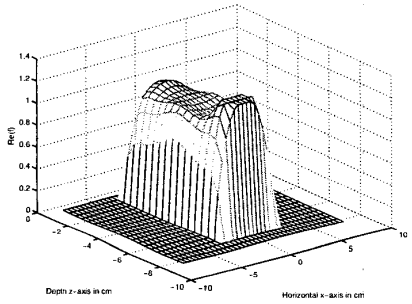

Figure 3. Plot of Re(f) vs. (x,z) for P2 with exact data

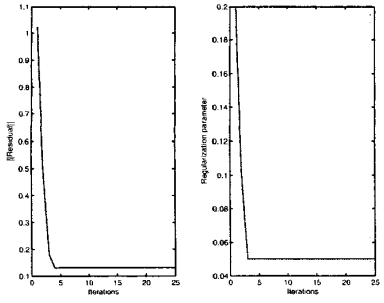

Figure 4. Plots of residual and regularization parameter vs. iteration for P2 with exact data

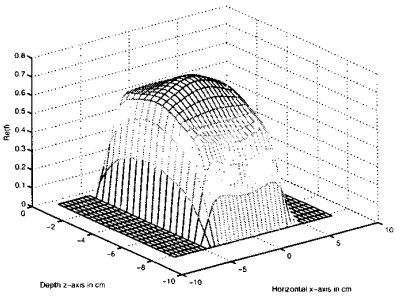

Figure 5. Plot of Re(f) vs. (x,z) for P1 with noisy data

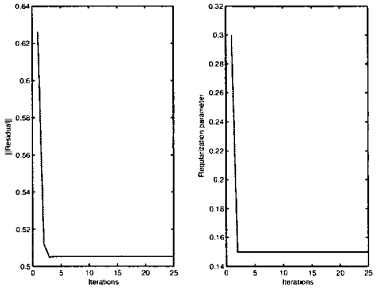

Figure 6. Plots of residual and regularization parameter vs. iteration for P1 with noisy data

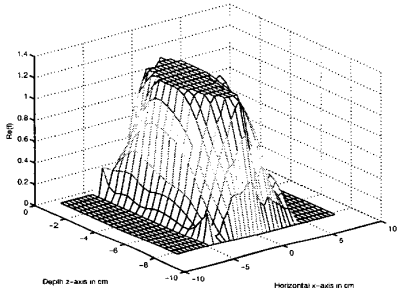

Figure 7. Plot of Re(f) vs. (x,z) for P2 with noisy data

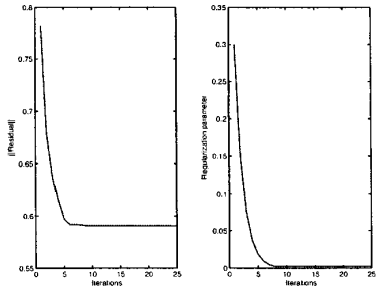

Figure 8. Plots of residual and regularization parameter vs. iteration for P2 with noisy data